

## Ocean surface wave dynamics off the southern tip of Indian mainland

Sanil Kumar V\*, Sivakrishnan K. K.

Ocean Engineering Division, CSIR-National Institute of Oceanography  
(Council of Scientific & Industrial Research), Dona Paula 403 004, Goa, India

\*Corresponding author: sanil@nio.org

### **Abstract**

Waves collected in the nearshore waters off the southern tip of the Indian mainland from February 2018 to January 2019 are used to examine the wave spectral characterization. The annual mean of the significant wave height (1.23m) in this area is slightly higher than that along the waters of the eastern Arabian Sea (0.9 to 1.1m), but the maximum value in an annual cycle (3.6m) is less than that (4.5 to 5m) found in those regions. Compared to other coastal locations around India, significant seasonal variations are not observed in the wave height at this location. A maximum of four wave systems are present in the study region. 76% of the surface height variance in the region results from swells from the south-southwest, and the balance is wind-seas from the west to the southeast. In a year, 72% of the time, single peak spectra are observed, majority of them are swell-dominated. The annual mean peak period and the wave energy potential of the area are larger than that available in the rest of the locations around the mainland of India. Also, the area is not subjected to high waves. Hence, it is an ideal location for installing wave energy converters.

**Keywords:** north Indian Ocean, surface waves, swells, wind-sea, spectral partitioning

## 1 Introduction

On the ocean surface, wind-generated waves are ubiquitous at the air-sea interface. Information on waves provides valuable insights for coastal management, maritime operations, and coastal engineering in the region. Wave data are required for planning coastal developments, designing offshore structures, and coastal protection measures. The waves in the ocean are the result of wind forcing, both local and remote forcing (Munk et al., 1963). Waves generated by the winds are able to travel large distances and reach distant shores. In the North Indian Ocean, the seasonal reversal of the monsoon winds (Wyrki, 1971) brings a shift in the wave direction (Kumar et al., 2012). During the Indian summer monsoon (June- September), the winds are from the southwest, while the winds are from the northeast in the post-monsoon (October- January). In the Arabian Sea, the winds blow strongly from May to September, due to the Findlater Jet with maximum wind stress magnitudes of about 6 dyne/cm<sup>2</sup>. The winds are very weak with maximum wind stress magnitudes of about 2 dyne/cm<sup>2</sup> during the transition months, March-April and October (Shetye et al., 1994). The earlier studies on the Indian shelf seas indicate that the waves generated in the Indian Ocean, the Southern Ocean, and the Atlantic Ocean characterize swell waves of the region (Samiksha et al., 2012; Remya et al., 2016; Amrutha et al., 2017; Naseef and Kumar, 2020 and references therein), whereas the locally generated wind waves constitute the wind-seas and the waves are influenced by the monsoon, low-level jets, tropical cyclones, and large scale ocean-atmosphere coupled processes such as Indian Ocean Dipole, El Niño Southern Oscillation and Boreal Summer Intra-Seasonal Oscillation (Anoop et al., 2015; Anoop et al., 2016; George and Kumar, 2019; Anoop et al., 2020; Joseph and Kumar, 2021; Aravind et al., 2023).

The complete depiction of waves at a location is given by the directional wave spectrum, and the types of waves present at a location are identified from the spectral partitioning of the directional spectrum. The spectral partitioning of the wave spectra was introduced by Gerling (1992), and improved by Hasselmann et al. (1996) and Hanson and Phillips (2001) using the watershed algorithm. Wang and Hwang (2001) proposed a separation method based on the steepness of wind-sea and swell and Hwang et al. (2012) improved this method based on a 1-D spectrum integration function, which solved the problem of swell overestimation, but this method is good for mixed or wind-sea-dominated sea states. Gilhousen and Hervey (2001) also estimated separation frequency based on a hypothesis that the steepness of swell is smaller than that of wind-sea, and the maximum steepness appears near the peak of wind-sea energy. Gilhousen and Hervey (2001) method is implemented by NOAA's National Data Buoy Center (NDBC). Based on the overshoot phenomenon in wind-generated waves, Chen et al. (2015) developed a method to extract wind-sea and swell from

the directional wave spectrum considering the observed data in the South China Sea. Portilla et al. (2009) modified the noise-removal scheme using a simple convolution kernel, which effectively solves the presence of small spurious partitions. Following Hanson and Phillips (2001) and Portilla et al. (2009), Douglas and Voulgaris (2019) developed a spectral partitioning algorithm. Watershed-based 2-D partitioning method (Douglas and Voulgaris, 2019) has proven itself as a sturdy and efficient means of spectral partitioning and is widely used and embedded in numerical wave models (e.g., WAVEWATCH III (Tolman, 1989)).

Villas Bôas et al. (2017) reported that the wave spectrum off the California coast consists of seven different wave systems, each one having characteristic directions and frequencies. In the eastern equatorial Pacific, wave spectral data consists of four wave systems (Portilla-Yandún et al., 2016). Studies based on the numerical model WAVEWATCH III, indicate that the waves in the deep waters off the southern coast of India are characterised by seven types of distinct clusters of wave systems (Amrutha and Kumar, 2021). The different wave systems during the tropical cyclone Kyarr are reported by Nair et al. (2022) through spectral partitioning of the measured 2-D wave spectra. Hsu et al. (2023) compared the performance of different wind-sea and swell separation methods for 1-D wave frequency spectrum during three historical Atlantic hurricanes, and also studied the model performance on 2-D directional wave spectrum. Hsu et al. (2023) found that the method proposed by Gilhousen and Hervey (2001) performed well during storm events and demonstrated the necessity of considering external data such as wind speed for sea-swell separation when available. In the central region of the west coast of India, three to four wave systems are observed (Sivakrishnan and Kumar, 2023).

Most of the earlier studies on surface waves in the coastal waters of India are in the central-eastern Arabian Sea (Kumar et al., 2003; Aboobacker et al., 2011; Kumar et al., 2012; Glejin et al., 2013; Nair and Kumar, 2017; Anusree and Kumar, 2023) and the western and northern Bay of Bengal (Sundar, 1986; Johnson et al., 2013; Nayak et al., 2013; Patra and Bhaskaran, 2016; Patra et al., 2016; Amrutha et al., 2017; Nair et al., 2019). The annual mean significant wave height at these locations is presented in Table 1. Studies on the wave characteristics in the coastal waters of the southern tip of India are limited.

In view of the above, an attempt is made in this article to study the wave characteristics in the coastal waters of the southern tip of India based on one-year-long measured wave data. The present study describes the seasonal variations in wave characteristics and identifies the predominant wave systems.

## 2. Data and methods

The present study uses measured wave data from February 2018 to January 2019 in the southern tip of India at Kolachel (latitude 8° 9.89' N; longitude 77° 14.92' E), at a water depth of 15 m (Fig. 1). The waves are measured with a surface following buoy (Datawell Directional Waverider). The buoy is moored using an anchor with a weight of 400 kg, a 30 m long rubber-cord of diameter 35 mm, and a 25 m long polypropylene rope of diameter 16 mm. The movement of the wave buoy is sampled at a rate of 3.84 Hz and is recorded onboard at a sampling frequency of 1.28 Hz. The data covering a period of 30 minutes are processed as one record. The resolution and accuracy of the heave measured are 0.01 m and 3%, respectively (Datawell, 2009). The wave spectrum is obtained from the data of heave through a fast Fourier transform. Data processing is through the use of the Waves21 software of Datawell (Datawell, 2009). The resolution of the spectral data from 0.025 Hz to 0.1 Hz is 0.005 Hz, and from 0.1 to 0.58 Hz, it is 0.01 Hz. Significant wave height ( $H_s$ ), spectral peak period ( $T_p$ ), mean wave period ( $T_{m02}$ ), and energy period ( $T_{m-10}$ ) are obtained every 30 minutes from the wave spectrum. The wave direction is based on circular moments following Kuik et al. (1988). The direction is the approaching direction at the peak frequency and is increasing clockwise with 0° as the north. The height ( $H$ ) and period ( $T$ ) of the individual wave are obtained from the zero up-crossing method (Tucker, 1991). The maximum height in a 30-minutes duration is maximum wave height ( $H_{max}$ ).

Following the Maximum Entropy Method (Lygre and Krogstad, 1986), the directional spectra,  $S(f, \theta)$ , are obtained. The method of Portilla et al. (2009) is used to distinguish the swells and wind-seas and calculate the separation frequency,  $f_c$ . The 1-D separation is carried out based on the hypothesis that the swell energy at the spectral peak cannot be higher than that of a Pierson-Moskowitz (PM) spectrum having the same frequency. At the same frequency, if the ratio between the peak spectral energy density of a record and the energy of a PM spectrum is above a threshold value of 1, then the record is classified as wind-sea, else it is considered as a swell. The swell parameters and wind-sea parameters are estimated for frequencies from 0.025 Hz to  $f_c$  and from  $f_c$  to 0.58 Hz.

A freak or rogue wave is identified when the abnormality Index (AI), the ratio between  $H_{max}$  and  $H_s$ , is more than 2 (Onorato et al., 2002). Gaps in the data in May are due to buoy maintenance. Wave power per crest length (kW/m) is obtained using the below expression (1).

$$P = \rho g \int_0^{2\pi} \int_0^{\infty} C_g(f, d) S(f, \theta) df d\theta \quad (1)$$

Where,  $\rho$  is seawater density ( $\text{kg/m}^3$ ),  $C_g$  is the group velocity (m/s),  $g$  is the gravitational acceleration ( $\text{m/s}^2$ ),  $d$  is the water depth (m), and  $\theta$  is the wave direction (deg).

The wave systems present in the study area are identified by spectral partitioning of the monthly directional wave spectra. Since the wind data was not available, the spectral partitioning algorithm used is that of Douglas and Voulgaris (2019) following Hanson and Phillips (2001) and Portilla et al. (2009). The directional wave spectrum is partitioned with the watershed algorithm after filtering using double convolution. For each partition, the peak frequency, peak direction, and peak energy are calculated. All the partitions within the wind region (frequency  $< 0.12$  Hz) are merged. The  $H_s$  and  $T_{m02}$  for each partition are estimated from spectral moments. The percentage contribution of swell (wind-sea) in a 30-minute record is estimated as the ratio of the swell (wind-sea)  $H_s$  and the total  $H_s$  of the respective record multiplied by 100.

### **3. Results and discussion**

#### **3.1. Variations in wave parameters**

Statistical analysis of the wave characteristics described in this section is based on the mean, maxima, and standard deviation. The annual mean value of  $H_s$  is 1.23 m with a standard deviation of 0.55 m, and the most energetic sea state is with  $H_s$  of 3.60 m and occurred on 16 July 2018 at 05:00 h during the monsoon (Table 2). The monthly average  $H_s$  ranged from 0.72 m in December to 2.12 m in July, with slightly higher monthly means ( $>1.6$  m) from May to August (Table 2). Intra-annual variability is observed with July exhibiting monthly mean wave powers thrice as large as those experienced in December. The daily variations are large, with a standard deviation of more than 0.35 m in May, July, and August. The maximum height of a single wave ( $H_{\text{max}}$ ) fluctuated from 0.6 to 6.0 m with an annual mean value of 1.9 m. Earlier studies have shown that waves in the eastern Arabian Sea (AS) have a strong seasonal variation (Kumar et al., 2012). In the present study area, seasonal average  $H_s$  are 1.07, 1.73, and 0.84 m in the pre-monsoon (February-May), monsoon, and post-monsoon (October-January), indicating that the inter-seasonal variations (42%) are less than those (76%) along the eastern AS (Kumar et al., 2014a).

The annual mean  $H_s$  observed (1.23 m) is higher than that reported (0.91 to 1.14 m) for other locations in the eastern AS (Table 1). In the study area, annually for 55% of the time,  $H_s$  exceeded 1 m. In April,  $H_s$  above 1.5 m are observed due to the long-period swells ( $T_p > 18$  s) (Figs. 2a and 2b). By 24 May, due to the monsoon influence,  $H_s$  increased from 1.5 m and reached 3.2 m by 28 May (Fig. 2). In the first week of June,  $H_s$  reduced to less than 2 m, and by 8 June,  $H_s$  started increasing from 2 to 2.8 m. The  $H_s$  at the study area is much less than the value (e.g., 4 m) measured in the same

period in the central-eastern AS at a location 810 km north of the study area. The high  $H_s$  in the central-eastern AS is due to the Findlater Jet (Findlater, 1969). Its influence on the southern tip is less, resulting in lower wave heights in the southern part of the eastern AS compared to the central part (Table 1). Anju and Kumar (2023) also observed that during June-July, the wave height is higher in the northern part of the west coast of India compared to the southern part.

Wave roses during three seasons and for the full year for  $H_s$  and  $T_p$  are presented in Fig. 3. Predominant waves are from the sector between south and southwest except during monsoon. During monsoon, most of the waves are from the sector between southwest and west. Wind-seas are from south-southeast and west during February-May and from southwest-west during the monsoon (Fig.3).

The peak wave period and associated wave direction are examined through scatter plots in different seasons (Fig. 4). The peak wave period has a wide range (4 to 22.2 s) with a mean value of 12.5 s, indicating the presence of short to long-period waves. Waves with periods in the range of 8 to 14 s had directions widely distributed (Fig. 4). Waves with larger  $T_p$  are from the south-southwest (direction  $<240^\circ$ ). Due to near resonance conditions, the long-period waves cause large heave motions of oil rigs and cause prose to offshore operations (Gjevik et al., 1988). Long-period waves and their orientation with moored vessels cause mooring line failure for ships berthed in open sea jetties (McComb et al., 2009). In the study area, around 3% of the time in a year, long-period waves ( $T_p > 18$  s), are recorded and these waves arrive from  $178^\circ$  to  $235^\circ$ .  $H_s$  of the long-period waves ranged from 0.6 to 3.1 m with an average height of 1.5 m. There is no specific season in which the long-period waves were observed, it was during 18-20 January, 21-23 April, 23 May, 23-30 July, 23-24 August, 26-28 September, 11 October, and 20 November. Over an annual cycle, the variation in the mean wave period is 3 to 11 s, with an annual average value of 6.4 s.

The swells and the wind-seas are separated to quantify their contribution to the wave characteristics in the study area. Swells contribute 76% of the surface height variance with a maximum  $H_s$  of 3.4 m with a mean  $H_s$  value of 1.1 m (Table 2). Wind-seas form the remaining 24% with a maximum value of 2.9 m and a mean value of 0.6 m. Wind-seas are relatively higher (29%) during February-May than the remaining period (23%). The predominance of swells over the wind-seas is similar to that observed in the eastern AS (Kumar et al., 2003; Glejin et al., 2013; Kumar et al., 2014a). The seasonal average swell contribution in the monsoon period is 77.2%, which is similar (70 to 79%) to that observed for other locations in the coastal waters of India (Kumar et al., 2014a). For a location in the Gulf of Mannar, Amrutha and Kumar (2017) observed that 53% of the

surface height variance is due to swells from the southeast and south and the balance is wind-seas from the southeast and east.

During the monsoon period, 54% of the time, intermediate-period waves ( $6 < T_p < 14$  s) are observed, while 18% of the time, short-period waves ( $T_p < 6$  s) and 28% of the time, long-period waves ( $T_p > 14$  s) are present. During post-monsoon, the intermediate-period, short-period, and long-period waves are 49%, 19%, and 32%, whereas, during the pre-monsoon, it is 48%, 24%, and 28% (Table 2).

The waves show a diurnal variation with the heights reaching highest in the late evening (19:30-23:30 LT, i.e., 14:00-18:00 GMT) in January, November, and December. From February to April, the maximum heights occurred between 09:00-12:00 GMT (Fig. 5). An inverse relation is observed between the wave period and the wave height due to the sea breeze-land breeze cycle, which is a common phenomenon in the nearshore areas of the tropics and subtropics and is pronounced during the non-monsoon months (Miller et al., 2003). Examination of the abnormality Index reveals that freak waves are present and their occurrence is 5.7%, 4.2%, and 6% during pre-monsoon, monsoon, and post-monsoon. Freak waves with higher heights ( $H_s > 2$  m) are present only in pre-monsoon and monsoon and their occurrence is 0.2 and 0.8% respectively (Fig. 6). Maximum significant wave height during freak waves is 3.1 and 2.9 m in pre-monsoon and monsoon and the significant steepness (corresponding to  $T_{m02}$ ) is 0.05 and 0.03. Earlier studies have shown that for narrow banded spectrum, freak waves occurred in sea states with significant steepness of more than 0.07 (Bitner-Gregersen and Gramstad, 2016), whereas in the present case, the spectrum is broad-banded with spectral with parameter between 0.82 and 0.90.

The mean value of wave power (8.8 kW/m) is higher than the median value (5.5 kW/m). The first and third quartile of the wave power is 3.1 and 11.5 kW/m. Wave power available in the study area is higher than that (7.9 kW/m) in the coastal waters of the central west coast of India. The maximum values of wave power are during the monsoon months of the year with average seasonal power of 15.6 kW/m and 6.2 kW/m during the pre-monsoon and 3.7 kW/m in the post-monsoon. The energy period (annual mean value is 9.7 s) is less than the spectral peak period (12.4 s) and hence estimation of wave power based on peak period (10.2 kW/m), which is a common practice in locations where the energy period is not available, will lead to 16% overestimation of the wave power. Recent studies based on reanalysis data also indicate that the coastal waters of the southern tip of India have a large wave energy potential compared to other locations in the coastal waters of India (Amrutha et al., 2020). Since the study area is also not subjected to high waves, it is an ideal location for installing wave energy converters. ERA5 data indicates that the maximum  $H_s$  from 2000

to 2017 at 8° N; 77.2° E, off the study area, is 3.3 m and the maximum individual wave height ( $H_{\max}$ ) is 6.0 m.

### 3.2 Wave spectra

A better understanding of different wave systems is achieved from the analysis of individual wave spectra. Measured wave data contains wind-sea or swell-dominated multi-peaked spectra, single-peaked swell, and single-peaked wind-sea (Table 3). Most of the data recorded are single-peaked spectra (72.2%), and these were mainly swells during 53.9% of the time and wind-seas during the remaining period. Most of the multi-peaked spectra (26.5%) were also swell-dominated (Table 3) indicating that overall, 80.4% of the spectra were swell-dominated. Amrutha and Kumar (2017) observed slightly higher multi-peaked spectra (58.5% of the time) in the east of the present location situated in the Gulf of Mannar. Globally, 75–85% of the ocean state at different locations are single peaked spectrum (Guedes Soares, 1991). The annual mean  $T_p$  (12.5 s) also indicates that the maximum spectral energy density is in the swell region. The annual mean  $T_p$  is highest in the coastal waters of the southern tip of India compared to that observed in the eastern AS (10-11.9 s), Gulf of Mannar (10.7-12.1 s) and northwestern Bay of Bengal (11.9-12.2 s) (Table 1).

The temporal variation of spectral energy distribution over a range of frequencies is studied with spectral energy density in the time-frequency plot (Fig. 7). The spectral energy density is normalized by the maximum value of the spectral energy density of the respective spectrum. Most of the time, spectral energy is predominantly in the frequency of swells (frequency bands 0.06-0.09 Hz) (Fig. 7).

The wave spectra clustered into various frequency bins indicate that the frequency peak of a large number of wave spectra (e.g., 44%) is between 0.08 and 0.1 Hz with an average  $H_s$  of 1.3 m and a mean period of 6.3 s (Table 4). 42% of the instantaneous observed snapshots of 2-D directional wave spectra are within peak frequencies of 0.06 and 0.08 Hz with a mean  $H_s$  of 1.1 m. Only during 0.05% of time wave spectra are with peak periods less than 5 s. The monthly averaged spectrum is mainly single-peaked in most of the months, except from February to April and October (Fig. 8a). The monthly average wave spectrum is swell-dominated in all the months. The peak frequency of the swell part of the monthly averaged wave spectrum varied from 0.07 to 0.095 Hz, with high values from June to August and low values during January, April, and September to October.

Wave systems with different peak frequencies generally come from different directions. Variations in directions of the monthly average spectrum are less for frequencies ranging from 0.05 to 0.1 Hz in all months. The mean wave direction shows large variation in the high-frequency band



(>0.15 Hz) in different months (Fig. 8b). During May to September, high-frequency waves are from 270 to 300°, during October and April, it is from 230 to 260° and in March and November-December, it is from 170 to 210°. The change in the high-frequency waves is mainly due to the change in the wind pattern from west-southwest to east-northeast caused by the southwest and northeast monsoons. Long-period swells ( $T_p > 14$  s) are mainly from 190 to 210°, and the intermediate-period waves ( $14 > T_p > 6$  s) are from 180 to 240°, while the wind-seas are from 150 to 280° (Fig. 8b). The spectral narrowness parameter ( $\nu$ ) varies from 0.42 to 0.99, with an average value of 0.66 indicating broad-banded wave spectrum. The values of the spectral peakedness parameter varied between 1 and 9 with a mean value of 2, and for high waves ( $H_s > 2$  m), the spectral peakedness parameter ranged from 1.6 to 2.6.

### 3.3. Spectral partitioning

The monthly mean directional wave spectra of each month from February 2018 to January 2019 is shown in Figure 9 and it indicates the spread of wave spectral energy in different frequencies and direction. Two well-separated peaks in spectral energy are observed from May to August due to the presence of monsoon waves from the southwest and the Southern Ocean swells from the south. The different wave systems obtained by spectral partitioning of the measured 2D wave spectra are presented in Figure 10. In the figures, partition 0 represents noise, partition 1 represents the wind-sea system, 2 represents the major swell system and the subsequent numbers represent other wave systems. A maximum of four wave systems are recorded during the study period. Figure 11 depicts the partial distribution of system-wide  $H_s$  and  $T_{m02}$  over a one-year period (February 2018 to January 2019). The highest (2.13 m) and lowest (0.71 m) total  $H_s$  are recorded in July and February, respectively. System 1 is a short-period (SP) wave system that exhibits fewer notable fluctuations throughout the period, except in May, when the  $H_s$  of System 1 is 0.80 m, accounting for approximately 23% of total  $H_s$ . System 2 is the dominating system throughout the year, composed of intermediate-period waves (IP) and sometimes SP. System 2 has the highest  $H_s$  in August (1.62 m) and the lowest in February (0.54 m). Except for May and February, System 2 is the largest contributor to total  $H_s$ , with a proportion of  $H_s$  to total  $H_s$  greater than 60% throughout the entire period. In August,  $H_s$  of System 2 contributed more than 90%. During June and July, the percentage of System 3  $H_s$  to total  $H_s$  is over 30%, and during all other months, when there are only three systems present, the partial to the total  $H_s$  ratio is only around 0.1. System 3 is made up of IP waves, yet it is around 4 s in February. System 4 appears in 6 months, with a  $H_s$  average of around 0.24 m and the maximum (0.37 m) occurs in July. System 4 appears to be the least significant, with partial

$H_s$  to the total  $H_s$  below 5%. During February, April and May System 4 consist of SP waves whereas in other months it is IP waves.

Amrutha and Kumar (2021) reported that the two systems with relatively high magnitude of energy are coming from the west. Spectral energy peak of the system from the west (System 3) starts to increase from May and diminishes as the monsoons progress, also the same pattern is observable in the case of  $H_s$  (Fig. 10). A low frequency (0.15-0.2 Hz) system from NW is present at locations in the western shelf seas, the same system is observed here as System 3 with wide directional spread and higher spectral energy peak (15-20  $m^2/Hz/deg$ ) during the monsoon period. A high-frequency system is also observed from the west having significant spectral energy (System 2). Even though Amrutha and Kumar (2021) observed two systems from the west with comparable  $H_s$  in deep-waters, in nearshore waters, System 2 had significantly higher  $H_s$  than System 3. Another system from the south with high frequency (0.1-0.2 Hz) is present with spectral energy peaks during July (10-15.1  $m^2/Hz/deg$ ). A system from SE directions with low directional spread is also observed during the pre- and post-monsoon periods. The system shows low spectral energy (0.1-0.5  $m^2/Hz/deg$ ). System 1 is locally generated waves. Swells due to monsoon winds and swells from the south Indian Ocean/Southern Ocean cause System 2.

#### **4 Concluding remarks**

One year of measured wave data using waverider buoy indicates that the annual average value of the significant wave height off the southern tip of Indian mainland is slightly higher than that along the coastal waters of the eastern AS. Over an annual cycle, 76% of the surface height variance in the study region is a result of the swells, and the balance is the wind-seas. Annually, 80.4% of the wave spectra are swell dominated. A maximum of four wave systems are observed in the study region. A large variation is observed in the direction of high-frequency waves in an annual cycle due to the change in the local wind direction. Throughout the year, intermediate period waves dominate the area. Land/sea breezes cause the diurnal variation. Energy period is less than the spectral peak period and hence estimation of wave power based on peak period led to 16% overestimation of the wave power. The region has larger wave energy potential compared to the rest of the locations around the mainland of India with least seasonal variations and are not subjected to extreme waves. Hence, coastal waters of the southern tip of the Indian mainland are an ideal location for installing wave energy converters.

## Acknowledgments

The authors thankfully acknowledge the CSIR, New Delhi, for facilitating the research work and the Ministry of Earth Sciences, New Delhi, for the financial support given to carry out the wave measurement. We thank TM Balakrishnan Nair, INCOIS, Hyderabad, for the guidance. Dr.S.Velvizhi, Fish For All Research and Training Centre, M.S.Swaminathan Research Foundation, Nagapattinam, Tamil Nadu, provided the support during data collection and the deployment of the buoy. Karunakar P, Salman Hussain A, Ramesh Kumar M, Jeyakumar C and Arun Nherakkol, staff members of Ocean Observation Group, Indian National Centre for Ocean Information Services (Ministry of Earth Sciences), Hyderabad are thanked for their contribution during data collection and deployment of the buoy. The authors thank both the reviewers for the comments and suggestions, which improved the content of the paper. This work has CSIR-NIO contribution number---

**Author contributions.** All authors contributed to the idea and scope of the paper. VSK performed the analyses and wrote the manuscript. KKS provided help with data analysis, discussed the results, and contributed to the writing of the paper.

**Competing interests.** The authors declare that they have no conflict of interest.

**Data availability:** The datasets analysed during the current study are available from the corresponding author on reasonable request. The data is also available at INCOIS ([http://www.incois.gov.in/Incois/info\\_insitu.jsp](http://www.incois.gov.in/Incois/info_insitu.jsp)).

## References

- Aboobacker, V. M., Rashmi, R., Vethamony, P., Menon, H. B., 2011. On the dominance of pre-existing swells over wind seas along the west coast of India. *Cont. Shelf Res.* 31(16), 1701-1712.
- Amrutha, M. M., Kumar, V. S., 2017. Observation of dominance of swells over wind seas in the coastal waters of the Gulf of Mannar, India. *Ocean Science* 13, 703–717, doi: 10.5194/os-13-703-2017
- Amrutha, M. M., Kumar, V. S., Bhaskaran, H., Naseef, T. M., 2019. Consistency of wave power at a location in the coastal waters of central eastern Arabian Sea. *Ocean Dynamics* doi: 10.1007/s10236-019-01267-1.
- Amrutha, M.M., Kumar, V.S., 2020. Changes in Wave Energy in the Shelf Seas of India during the Last 40 Years Based on ERA5 Reanalysis Data. *Energies.* 13, 115. doi:10.3390/en13010115.
- Amrutha, M.M., Kumar, V.S., 2021. Identification of wave systems in the multimodal sea state along the Indian shelf seas, *Ocean Dynamics*, <https://doi.org/10.1007/s10236-021-01456-x>.
- Anju, T. M., Kumar, V.S., 2023. Steepness of surface gravity waves measured in the eastern Arabian Sea during peak monsoon months, *Ocean Engineering* 280, Article number 114900. <https://doi.org/10.1016/j.oceaneng.2023.114900>.

- Anoop, T.R., Kumar, V.S., Shanas, P.R., Johnson, G., 2015. Surface wave climatology and its variability in the North Indian Ocean based on ERA-Interim reanalysis. *J Atmos Ocean Technol* 32 (7):1372–1385. <https://doi.org/10.1175/JTECH-D-14-00212.1>.
- Anoop, T.R., Kumar, V.S., Shanas, P.R., Johnson, G., Amrutha, M.M., 2016. Indian Ocean Dipole modulated wave climate of eastern Arabian Sea, *Ocean Science*, 12, 369-378, doi:10.5194/osd-12-2473-2015.
- Anoop, T.R., Shanas, P.R., Aboobacker, V.M., Sanil Kumar, V., Nair, L.S., Prasad, R., Reji, S., 2020. On the generation and propagation of Makran swells in the Arabian Sea. *Int. J. climatology* 40 (1): 585-593. <https://doi.org/10.1002/joc.6192>.
- Anusree, A., Kumar, V.S., 2023. Variations in short-term statistics of waves observed in the coastal waters of the eastern Arabian Sea, *Ocean Engineering* 281, Article number 114824. <https://doi.org/10.1016/j.oceaneng.2023.114824>.
- Aravind, P., Kumar, V.S., Shanas, P R., Joseph, D., 2023. Interannual variability of wind-wave climate during two types of ENSO events in the Indian Ocean, *International Journal of Climatology* (under review).
- Bitner-Gregersen, E.M., Gramstad, O., 2016. Rogue waves: impact on ships and offshore structures. *Det Norske Veritas Germanischer Lloyd Strategic Research and Innovation Position Paper 5–2015* 60.
- Chen, Z., Zhang, L., Zhao, C., Chen, X., Zhong, J., 2015. A Practical Method of Extracting Wind Sea and Swell from Directional Wave Spectrum. *J. Atmos. Oceanic Technol.*, 32, 2147–2159, <https://doi.org/10.1175/JTECH-D-15-0092.1>.
- Datawell, 2009. *Datawell Waverider Reference Manual*, Datawell BV oceanographic instruments, The Netherlands, pp 123.
- Douglas, C., Voulgaris, G., 2019. WavePART: MATLAB(r) software for the partition of directional ocean wave spectra. *Zenodo*. doi:10.5281/zenodo.2638500.
- Findlater, J., 1969. A major low-level air current near the Indian Ocean during the northern summer. *Quart. J. Roy. Meteor. Soc.* 95, 362-380. doi:10.1002/qj.49709540409.
- George, J., Kumar, V.S., 2019. Long-term variations in nearshore wave climate and littoral drift at Ganpatipule coast, eastern Arabian Sea and its link to Pacific climate variability. *Journal of Geophysical Research, Oceans*. doi: 10.1029/2018JC014900.
- Gerling, T.W., 1992. Partitioning sequences and arrays of directional ocean wave spectra into component wave systems. *J. Atmos. Ocean. Technol.* 9 (4), 444–458.
- Gilhousen, D.B., Hervey, R., 2001. Improved Estimates of Swell from Moored Buoys. 387–393. [http://dx.doi.org/10.1061/40604\(273\)40](http://dx.doi.org/10.1061/40604(273)40), URL: <https://ascelibrary.org/doi/abs/10.1061/40604>
- Gjevik, B., Krogstad, H., Lygre, A., Rygg, O., 1988. Long period swell wave events on the Norwegian Shelf. *Journal of Physical Oceanography*, 18, 724–737.

- Glejin, J., Kumar, V.S., Amrutha, M. M., Singh, J., 2016. Characteristics of long-period swells measured in the in the near shore regions of eastern Arabian Sea, *International J. Naval Architecture and Ocean Eng.* 8, 312-319. doi: 10.1016/j.ijnaoe.2016.03.008.
- Gowthaman, R., Kumar, V. S., Dwarakish, G. S., Soumya, S. M, Singh, J., Kumar, K. A., 2013. Waves in Gulf of Mannar and Palk Bay around Dhanushkodi, Tamil Nadu, India. *Current Science* 104(10), 1431-1435.
- Guedes Soares, C., 1991. On the occurrence of double peaked wave spectra. *Ocean Eng.* 18 (1–2):167–171.
- Hanson, J.L., Phillips, O.M., 2001. Automated Analysis of Ocean Surface Directional Wave Spectra. *Journal of Atmospheric and Oceanic Technology* 18, 277–293. [https://doi.org/10.1175/1520-0426\(2001\)018<0277:aaosd>2.0.co;2](https://doi.org/10.1175/1520-0426(2001)018<0277:aaosd>2.0.co;2).
- Hasselmann, S., Brüning, C., Hasselmann, K., Heimbach, P., 1996. An improved algorithm for the retrieval of ocean wave spectra from synthetic aperture radar image spectra. *J. Geophys. Res.: Oceans* 101 (C7), 16615-16629.
- Hwang, P.A., Ocampo-Torres, F.J., García-Nava, H., 2012. Wind Sea and swell separation of ID wave spectrum by a spectrum integration method. *J. Atmos. Ocean. Technol.* 29, 116–128, <https://doi.org/10.1175/JTECH-D-11 - 00075.1>.
- Hsu, Chu-En, Christie A. Hegermiller, John C. Warner, Maitane Olabarrieta, 2023. Ocean Surface Gravity Wave Evolution during Three Along-Shelf Propagating Tropical Cyclones: Model's Performance of Wind-Sea and Swell. *Journal of Marine Science and Engineering* 11, no. 6: 1152. <https://doi.org/10.3390/jmse11061152>.
- Johnson, G., Kumar, V. S., Nair, T. M. B., 2013. Monsoon and cyclone induced wave climate over the near shore waters off Puduchery, south western Bay of Bengal. *Ocean Eng.* 72, 277–286. doi:10.1016/j.oceaneng.2013.07.013.
- Joseph, D., Kumar, V.S., 2021. Response of ocean surface waves to the co-occurrence of Boreal Summer Intra-Seasonal Oscillation and El Niño Southern Oscillation. *Climate Dynamics* 57:1155–1171, <https://doi.org/10.1007/s00382-021-05763-3>
- Kuik, A. J., Vledder, G. P., Holthuijsen, L. H., 1988. A method for the routine analysis of pitch and roll buoy wave data. *J. Phys. Oceanogr.* 18, 1020-1034.
- Kumar, V.S., Anand, N. M., Kumar, K. A., Mandal, S., 2003. Multi peakedness and groupiness of shallow water waves along Indian coast. *J. Coastal Res.* 19, 1052-1065.
- Kumar, V.S., Shanas, P.R, Dubhashi, K.K, 2014a, Shallow water wave spectral characteristics along the eastern Arabian Sea, *Natural Hazards* 70, 377–394, doi:10.1007/s11069-013-0815-7
- Kumar, V.S., Dubhashi, K. K., Nair, T. M. B., 2014b. Spectral wave characteristics off Gangavaram, Bay of Bengal. *J. Oceanography* 70(3), 307-321. doi:10.1007/s10872-014-0223-y.
- Kumar, V.S., Glejin J., Dora, G. U., Sajiv, P. C., Singh, T., Pednekar, P., 2012. Variations in near shore waves along Karnataka, west coast of India. *J. Earth System Science* 121, 393-403. doi:10.1007/s12040-012-0160-3.

- Lygre, A., Krogstad, H. E., 1986. Maximum entropy estimation of the directional distribution in ocean wave spectra. *J. Phys. Oceanogr.* 16(12), 2052–2060.
- McComb, P., Johnson, D., Beamsley, B., 2009. Numerical model study to reduce swell and long wave penetration to Port Geraldton. *Proceedings of the 2009 Pacific Coasts and Ports Conference*, Wellington, New Zealand.
- Miller, S.T., Keim, B.D., Talbot, R.W., Mao, H., 2003. Sea breeze: Structure, forecasting, and impacts. *Reviews of geophysics*, 41, 1-31.
- Munk, W. H., Miller, G. R., Snodgrass, F. E., Barber, N., 1963. Directional recording of swell from distant storms. *Philosophical Transactions of the Royal Society of London, Series A*, 255 (1062): 505–584.
- Nair, M.A., Amrutha, M.M., Kumar, V.S., 2022. Spectral wave characteristics in the coastal waters of the central west coast of India during tropical cyclone Kyarr, *Ocean Dynamics*, 72:151–168, <https://doi.org/10.1007/s10236-022-01496-x>.
- Nair, M.A., Kumar, V.S., 2017. Wave spectral shapes in the coastal waters based on measured data off Karwar on the west coast of India. *Ocean Science*. 13, 365–378. doi:10.5194/os-13-365-2017.
- Nair, M.A., Kumar, V.S., Amrutha, M.M., Murty, V.S.N., 2019. Features of locally and remotely generated surface gravity waves in the inner-shelf region of north-western Bay of Bengal, *International Journal of Climatology*, 39:1644-1664 doi: 10.1002/joc.5907.
- Nair, M.A., Kumar, V.S., Amrutha, M.M., 2018. Spectral wave characteristics in the nearshore waters of northwestern Bay of Bengal, *Pure and Applied Geophysics*, 175, 3111-3136. doi.org/10.1007/s00024-018-1838-5.
- Naseef, T.M., Kumar, V.S., 2020. Climatology and trends of the Indian Ocean surface waves based on 39-year long ERA5 reanalysis data, *International Journal of Climatology*, 40, 979-1006, doi.org/10.1002/joc.6251.
- Nayak, S., Bhaskaran, P. K., Venkatesan, R., Dasgupta, S., 2013. Modulation of local wind waves at Kalpakkam from remote forcing effects of Southern Ocean swells. *Ocean Engg.* 64, 23-35.
- Onorato, M., Osborne, A. R., Serio, M., 2002. Extreme wave events in directional, random oceanic sea states, *Phys. Fluids*, 14, 3–6, <https://doi.org/10.1063/1.1453466>, 2002.
- Patra, A., Bhaskaran, P. K., 2016. Temporal variability in wind-wave climate and its validation with ESSO NIOT wave atlas for the head Bay of Bengal. *Clim. Dyn.* 1-18. doi:10.1007/s00382-016-3385-z
- Patra, S. K., Mishra, P., Mohanty, P. K., Pradhan, U. K., Panda, U. S., Murthy, M. V. R., Kumar, V. S., Nair, T. M. B., 2016. Cyclone and monsoonal wave characteristics of northwestern Bay of Bengal: long-term observations and modelling. *Natural Hazards* 82, 1051–1073. doi:10.1007/s11069-016-2233-0.
- Portilla, J., Ocampo-Torres, F.J., Monbaliu, J., 2009. Spectral Partitioning and Identification of Wind Sea and Swell. *Journal of Atmospheric and Oceanic Technology* 26, 107–122. <https://doi.org/10.1175/2008jtecho609.1>.

- Portilla-Yandún, J., Salazar, A., Cavaleri, L., 2016. Climate patterns derived from ocean wave spectra. *Geophysical Research Letters*, 43, 11,736–11,743. <https://doi.org/10.1002/2016GL071419>.
- Remya, P. G., Vishnu, S., Praveen Kumar, B., Balakrishnan Nair, T. M., Rohith, B., 2016. Teleconnection between the North Indian Ocean high swell events and meteorological conditions over the Southern Indian Ocean. *J. Geophys. Res. Oceans* 121, 7476–7494. doi:10.1002/2016JC011723.
- Samiksha, S.V., Vethamony, P., Aboobacker, V.M. Rashmi, R., 2012. Propagation of Atlantic Ocean swells in the north Indian Ocean: A case study. *Natural Hazards and Earth System Sciences* 12, 3605-3615.
- Shetye, S.R., Gouveia, A.D., Shenoi, S.S.C., 1994. Circulation and water masses of the Arabian Sea, In: Lal,D. (Ed.), *Proceedings of the Indian Academy of Sciences*, Lotus Printers, New Delhi, India, pp. 9–25.
- Sivakrishnan, K.K., Kumar, V.S., 2023. Seasonal cycle of wave systems in a multimodal sea state in the coastal waters of eastern Arabian Sea, *Journal of Operational Oceanography* (under review).
- Sundar, V., 1986. Wave characteristics off the South East Coast of India. *Ocean Engg.* 13(4), 327-338.
- Tucker, M.J., 1991. *Waves in ocean engineering: measurement, analysis, interpretation*. Ellis Horwood, Chichester, UK. 431 pp.
- Villas Bôas, A. B., Gille, S. T., Mazloff, M. R., Cornuelle, B. D., 2017. Characterization of the deep-water surface wave variability in the California Current region. *Journal of Geophysical Research: Oceans*, 122, 8753–8769. <https://doi.org/10.1002/2017JC013280>.
- Wyrtki, K., 1971. *Oceanographic atlas of the international Indian Ocean expedition*. Washington, DC. National Science Foundation.

Table 1. Studies on waves in Indian waters based on measured wave data covering 1 year and above

Location	Position	Water depth (m)	Period of data used	Data (%)	Annual average $H_s$ (m)	Annual average $T_p$ (s)	Reference
Versova, north-north-eastern Arabian Sea	19.1300° N; 72.7400° E	15	1 Jan 2017- 31 Dec 2017	100	0.91	10.0	Kumar et al. (2018)
Ratnagiri, eastern Arabian Sea	16.980° N; 73.258° E	13	1 Jan 2011- 31 Dec 2011	99.98	1.14	10.1	Amrutha et al. (2019)
Vengurla, eastern Arabian Sea	15.842° N 73.563° E	15	1 Sep 2014 - 31 Aug 2015	99.95	0.94	11.6	George et al. (2020)
Karwar, eastern Arabian Sea	14.822° N; 74.052° E	15	1 Jan 2011- 31 Dec 2011	99.98	1.13	11.5	Nair and Kumar (2017)
Honnavar, eastern Arabian Sea	14.304° N; 74.391° E	9	1 Jan 2011- 31 Dec 2011	95.65	1.05	11.9	Amrutha and Kumar (2016)
Tuticorin, Gulf of Mannar	8.8811° N; 78.2956° E	12	1 May 2015- 30 Apr 2016	99.94	0.84	12.1	Amrutha and Kumar (2017)
Off Dhanushkodi, Gulf of Mannar	9.113° N; 79.407° E	12	9 Feb 2010- 31 Mar 2011	90.54	0.90	10.7	Gowthaman et al. (2013)
Off Dhanushkodi, Palk Bay	9.319°N; 79.434°E	12	9 Feb 2010- 31 Mar 2011	96.52	0.55	3.3	Gowthaman et al. (2013)
Puducherry, western Bay of Bengal	11.924° N; 79.851° E	15	1 Jan 2010- 31 Dec 2010	99.98	0.70	8.0	Johnson et al. (2013)
Gangavaram, northwestern Bay of Bengal	17.633° N; 83.267° E	18	1 Jan 2010- 31 Dec 2010	97.48	1.02	11.9	Kumar et al. (2014b)
Visakhapatnam, north western Bay of Bengal	17.705° N; 83.328° E	15	1 Mar 2015- 29 Feb 2016	100	1.04	12.4	Nair et al. (2019)
Gopalpur, northern Bay of Bengal	19.282° N; 84.964° E	15	1 Jan 2015- 31 Dec 2015	99.99	1.00	12.2	Nair et al. (2018)



Table 2. Statistics of each month: mean value, standard deviation and maximum of significant wave height along with swell and wind-sea percentage and its heights in the measured data

Month	Mean (m)	Standard deviation (m)	Maximum (m)	Average $T_p$ (s)	No. of data	Swell (%)	Average $H_s$ of swell (m)	Wind- sea (%)	Average $H_s$ of wind- sea (m)
February 2018	0.72	0.06	0.87	11.3	125	67.0	0.59	33.0	0.41
March 2018	0.85	0.18	1.42	12.2	1488	70.6	0.71	29.4	0.44
April 2018	1.03	0.25	2.25	13.0	1408	79.0	0.91	21.0	0.45
May 2018	1.62	0.54	3.24	12.1	762	60.3	1.26	39.7	0.95
June 2018	1.86	0.28	2.78	11.0	1260	72.1	1.57	27.9	0.96
July 2018	2.12	0.40	3.60	13.1	1488	82.3	1.93	17.7	0.87
August 2018	1.66	0.36	3.02	11.5	1488	76.1	1.44	23.9	0.79
September 2018	1.27	0.18	1.81	13.6	1440	77.4	1.12	22.6	0.59
October 2018	1.08	0.26	2.36	12.4	1488	76.2	0.94	23.8	0.52
November 2018	0.77	0.12	1.19	11.9	1440	76.3	0.67	23.7	0.37
December 2018	0.72	0.17	1.25	12.3	1485	76.9	0.64	23.1	0.32
January 2019	0.75	0.16	1.43	13.8	1271	78.2	0.67	21.8	0.33
Pre- monsoon	1.07	0.42	3.24	12.5	3783	71.5	0.89	28.5	0.55
monsoon	1.73	0.45	3.60	12.4	5676	77.2	1.51	22.8	0.80
Post- monsoon	0.84	0.24	2.36	12.6	5684	76.9	0.73	23.1	0.39
Annual average	1.23	0.55	3.60	12.5	15143	75.6	1.06	24.4	0.58

Table 3. Percentage of single-peaked and multi-peaked wave spectra in different months along with classification as wind-sea, swell or mixed based on spectral peak period

Month	Single-peak (%)			Multi-peak (%)		
	Total	Wind-sea dominated ( $T_p < 8$ s)	Swell dominated ( $T_p > 8$ s)	Total	Wind-sea dominated ( $T_p < 8$ s)	Swell dominated ( $T_p > 8$ s)
January	88.99	0.00	88.99	11.01	0.00	11.01
February	89.60	0.00	89.60	10.40	0.00	10.40
March	69.02	0.07	68.95	30.98	0.94	30.04
April	86.86	0.14	86.72	13.14	0.00	13.14
May	35.70	22.57	13.12	64.30	12.07	52.23
June	60.24	56.83	3.41	39.76	0.79	38.97
July	79.30	68.28	11.02	20.70	0.00	20.70
August	73.59	53.16	20.43	26.41	0.13	26.28
September	71.25	9.93	61.32	28.75	0.00	28.75
October	56.05	6.52	49.53	43.95	2.08	41.87
November	78.26	0.00	78.26	21.74	0.07	21.67
December	76.97	0.00	76.97	23.03	0.47	22.56
Annual average	72.15	18.22	53.93	27.85	1.35	26.49

Table 4. Average wave parameters and amount of wave spectra in different spectral peak frequencies

Peak frequency ( $f_p$ ) range (Hz)	Number of wave spectra	Percentage of wave spectra	$H_s$ (m)	$T_{m02}$ (s)	Peak wave period (s)
$0.04 < f_p \leq 0.05$	102	0.67	1.48	7.98	20.24
$0.05 < f_p \leq 0.06$	1092	7.21	1.44	6.99	17.18
$0.06 < f_p \leq 0.07$	3005	19.84	1.16	6.44	14.67
$0.07 < f_p \leq 0.08$	3370	22.25	1.05	6.27	12.93
$0.08 < f_p \leq 0.10$	6646	43.89	1.30	6.31	10.86
$0.10 < f_p \leq 0.15$	892	5.89	1.25	5.97	8.75
$0.15 < f_p \leq 0.20$	28	0.18	1.25	5.01	5.93
$0.20 < f_p \leq 0.30$	8	0.05	1.13	3.95	4.39

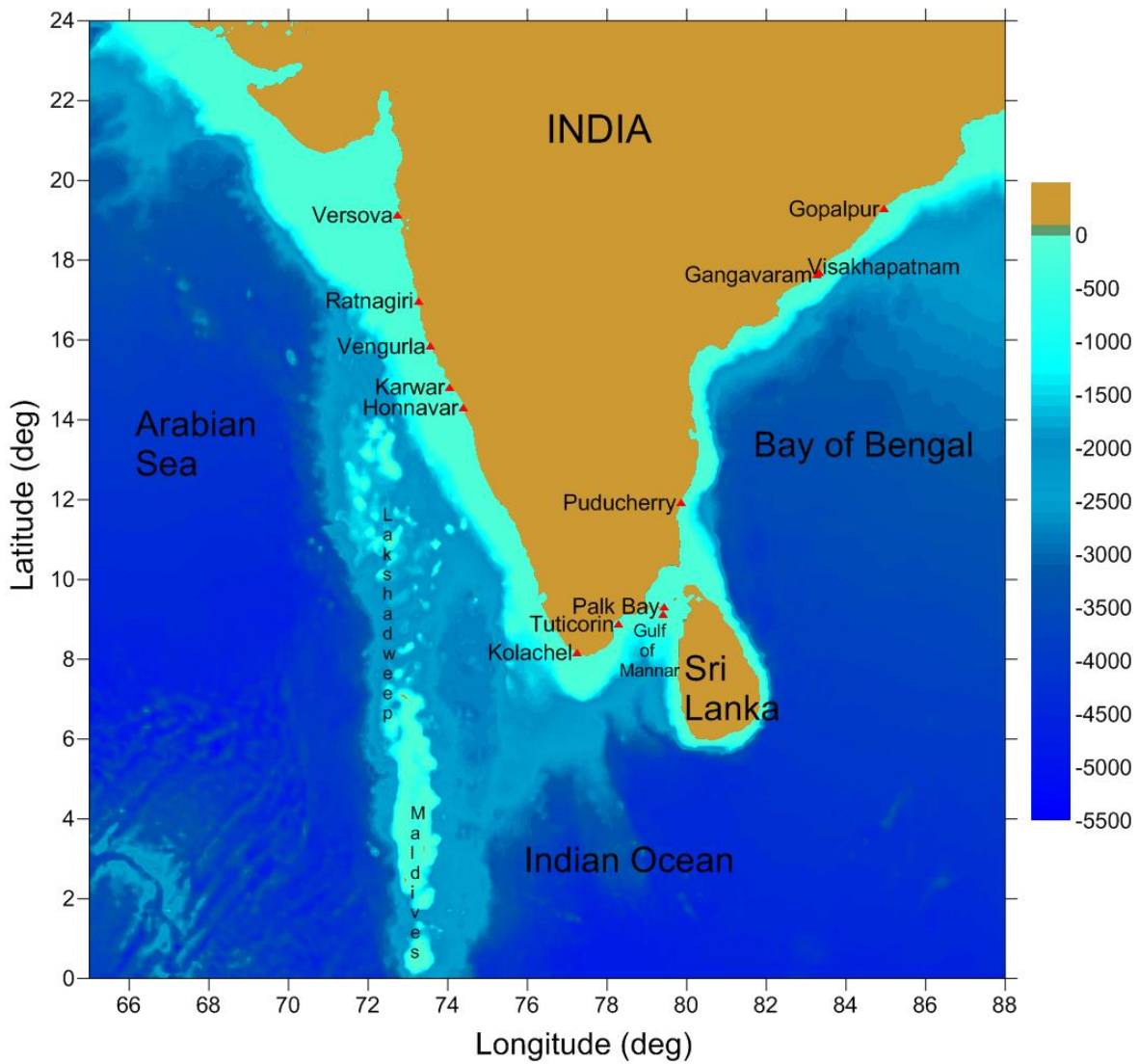


Figure 1. Map showing the buoy location off the southern tip of Indian mainland (off Kolachel) used in the present study. The colour contour indicates the water depth in metre. The wave buoy locations mentioned in Table 1 are also indicated in the figure

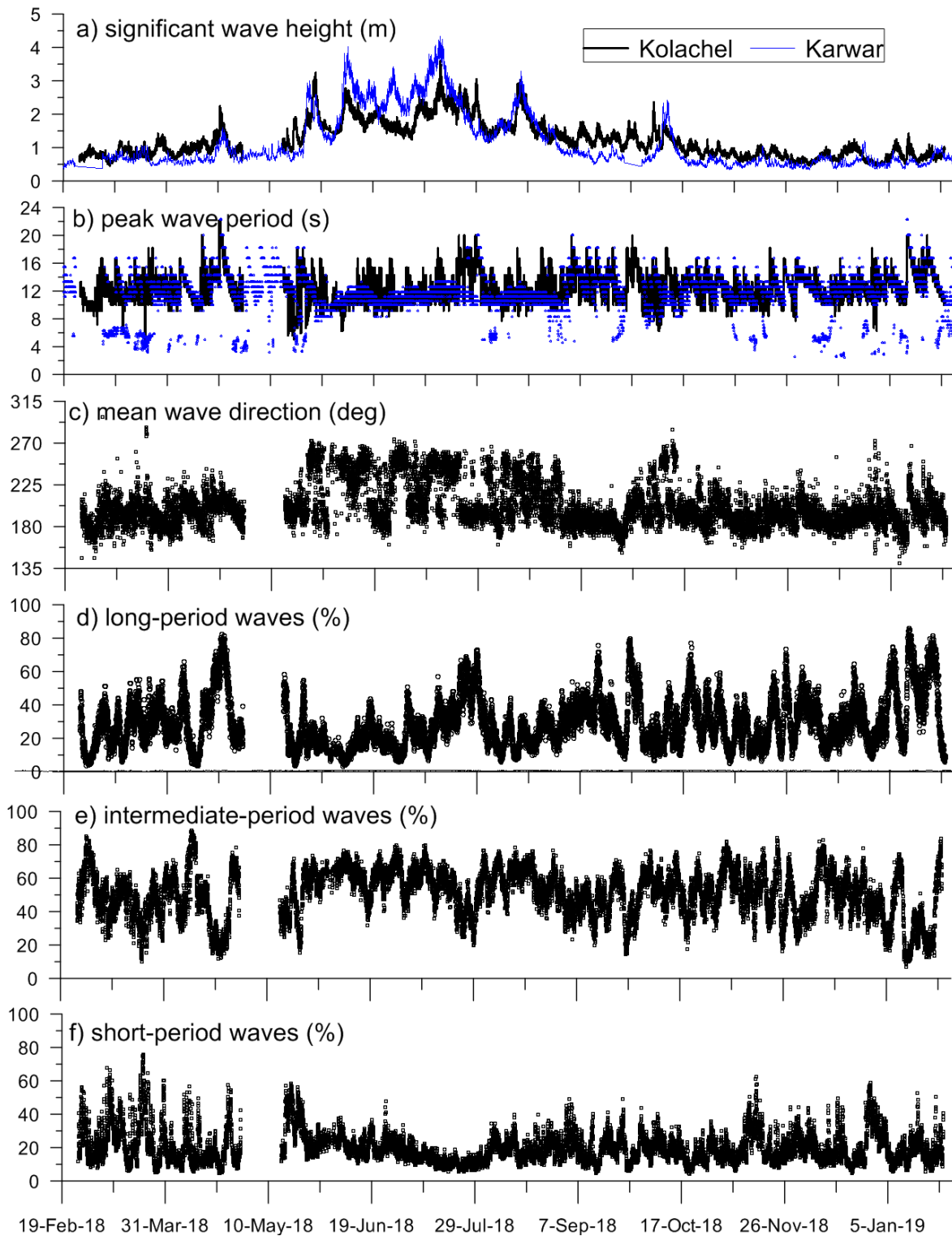


Figure 2. Time series plot of a) significant wave height, b) peak wave period, c) mean wave direction, d) percentage of long-period waves, e) percentage of intermediate-period waves and f) percentage of short-period waves. Significant wave height and peak wave period at Karwar, a location 810 km north of the study area is also shown in Figure 2a and 2b

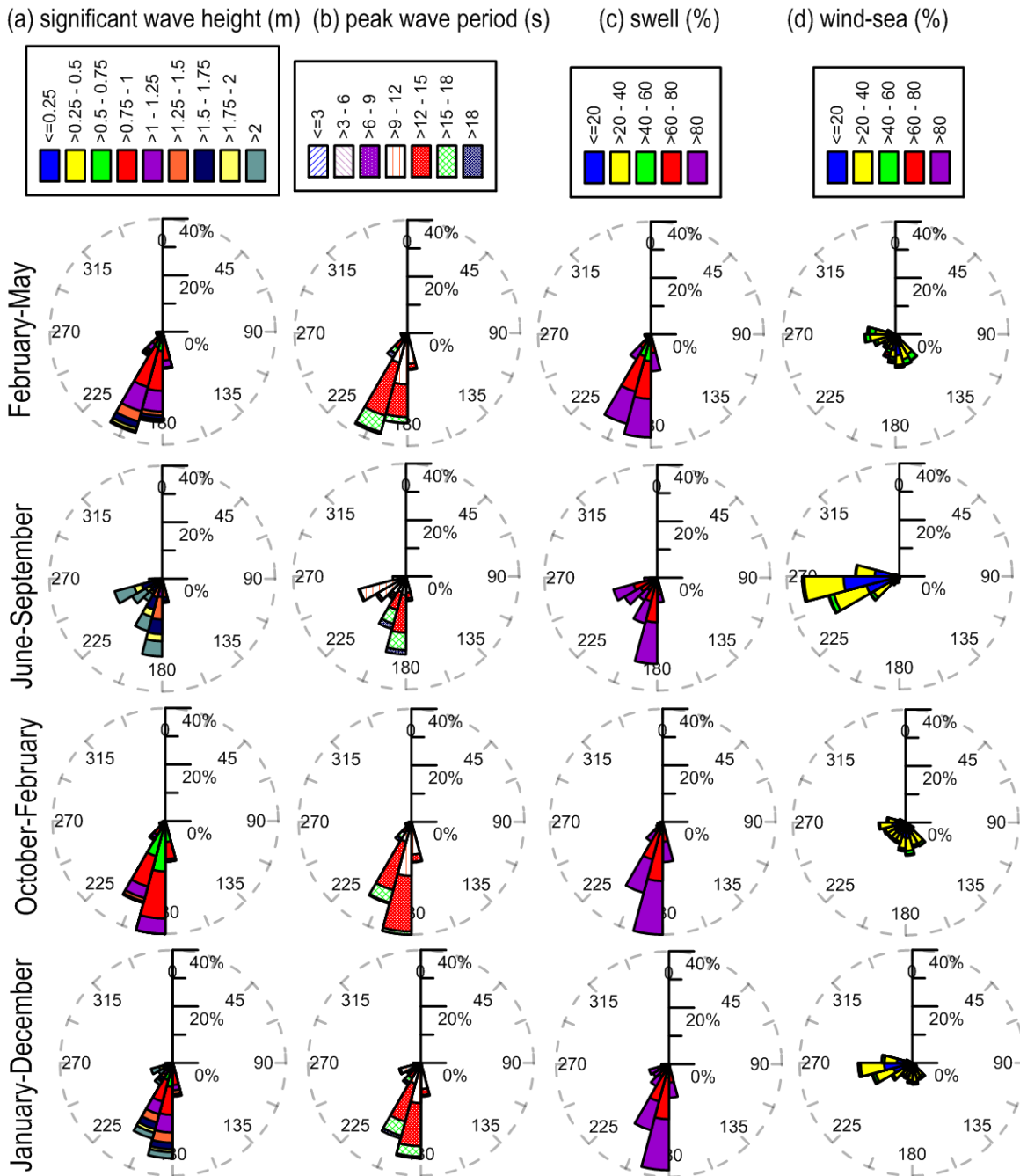


Figure 3. Wave roses during different periods from February 2018 to January 2019 (a) significant wave height and mean wave direction, (b) peak wave period and mean wave direction, (c) percentage of swell in the measured data and mean wave direction, (d) percentage of wind-sea in the measured data and mean wave direction. The plots represent the direction where the waves come from. The radius of the figure indicates the percentage of the time

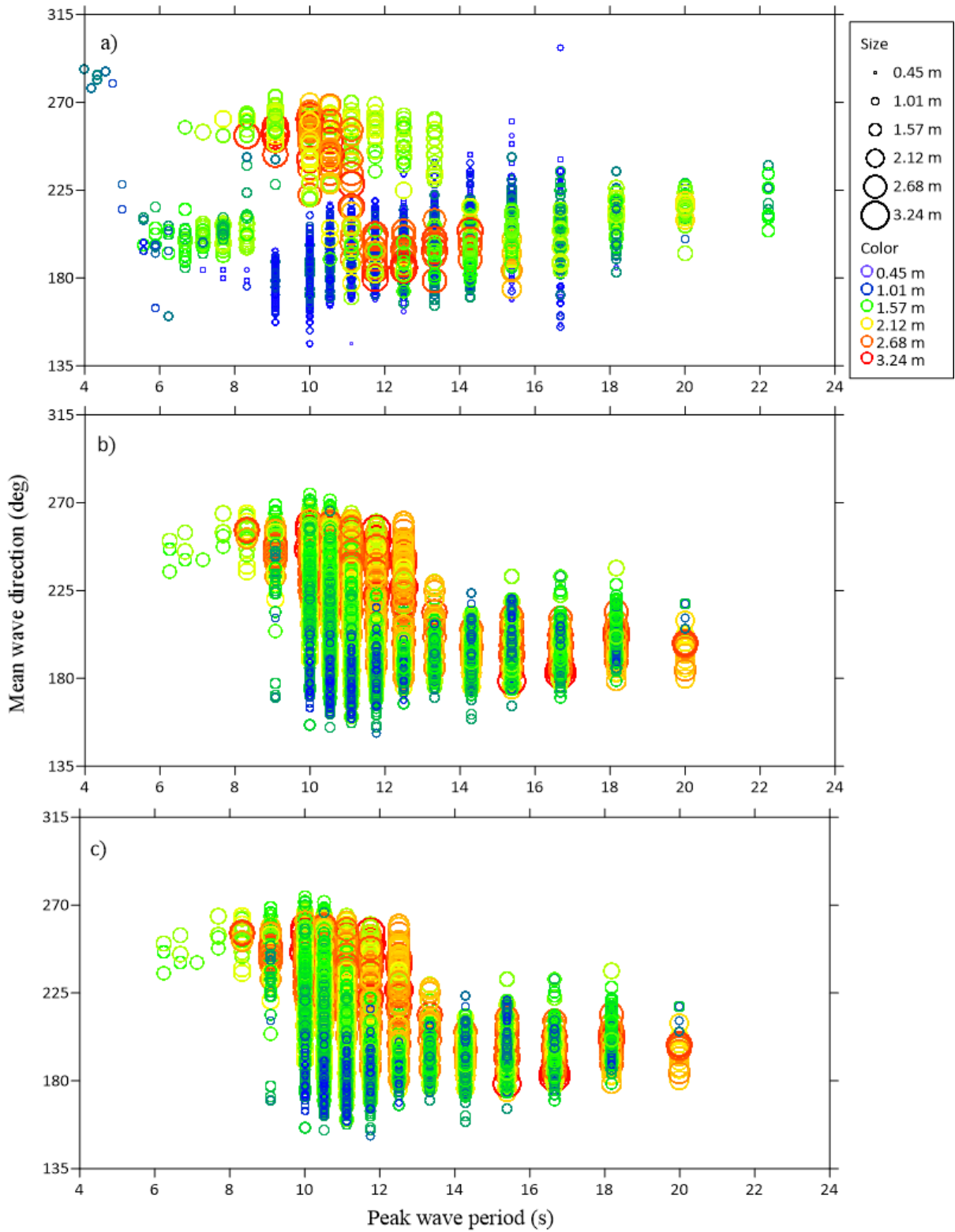


Figure 4. Scatter diagram showing mean wave direction and peak wave period in different seasons (a) February-May, (b) June-September, (c) October-January. The size and colour of the bubble is proportional to the significant wave height value

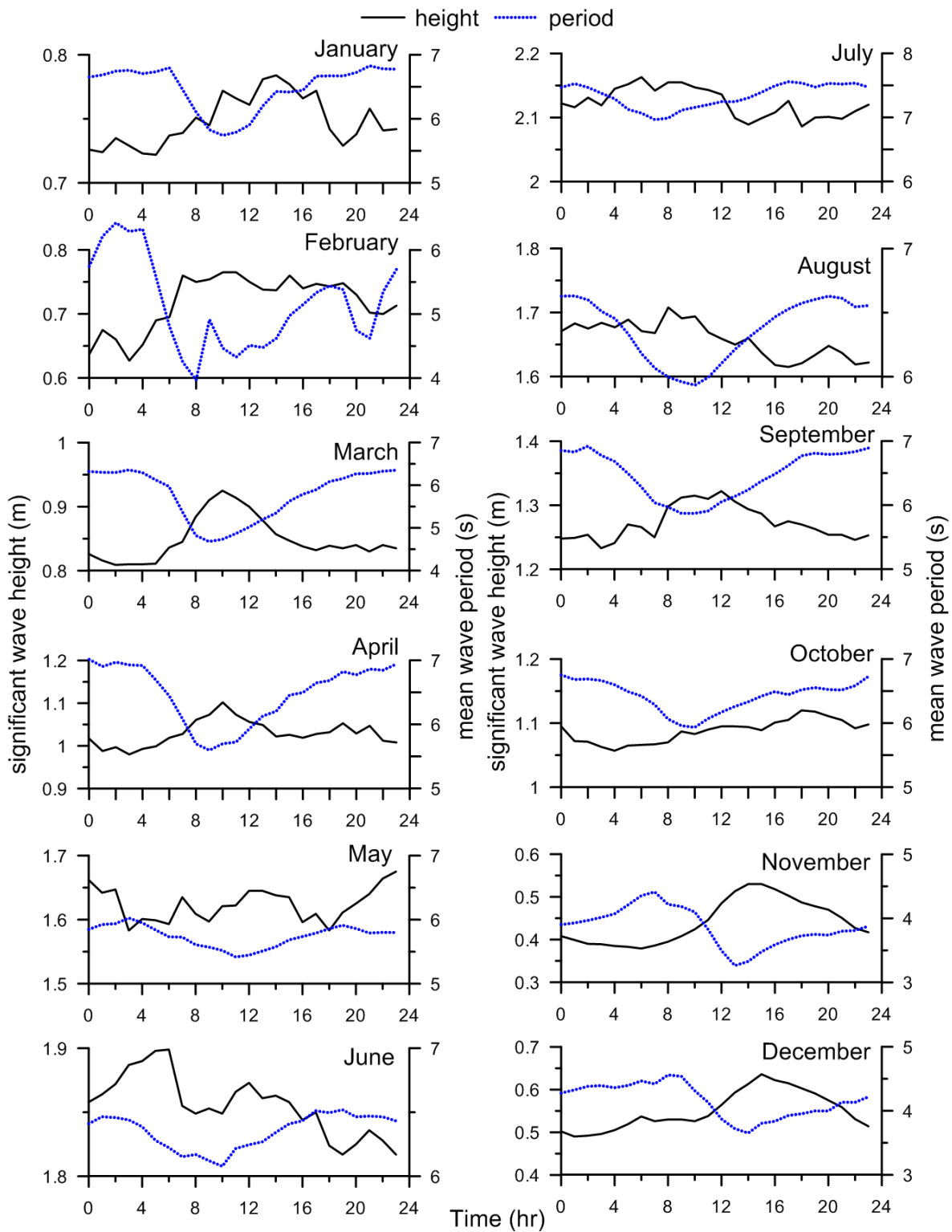


Figure 5. Variation of hourly averaged significant wave height and mean wave period in different months



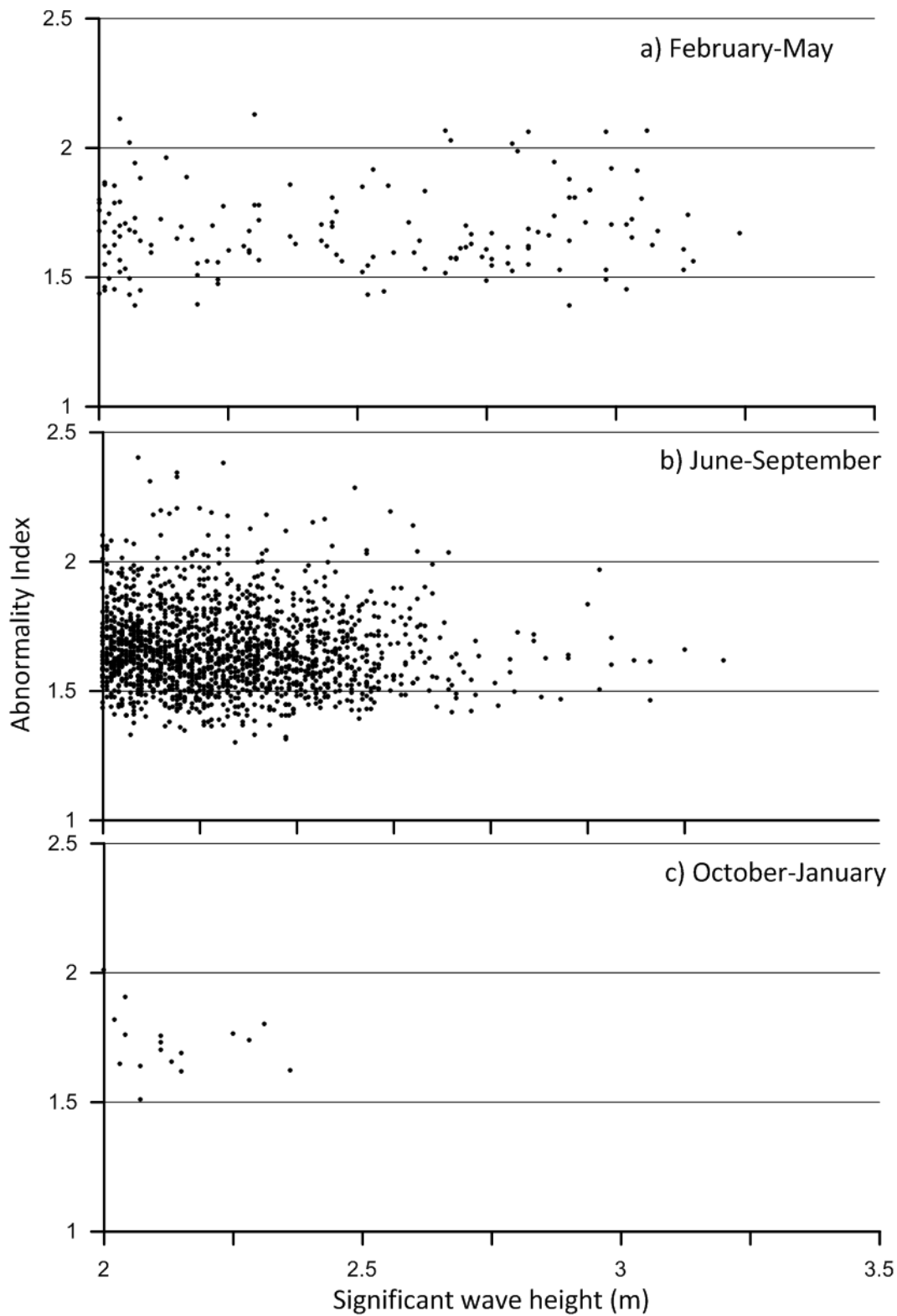


Figure 6. Abnormality Index for significant wave height more than 2 m during different seasons a) pre-monsoon, b) monsoon and c) post-monsoon

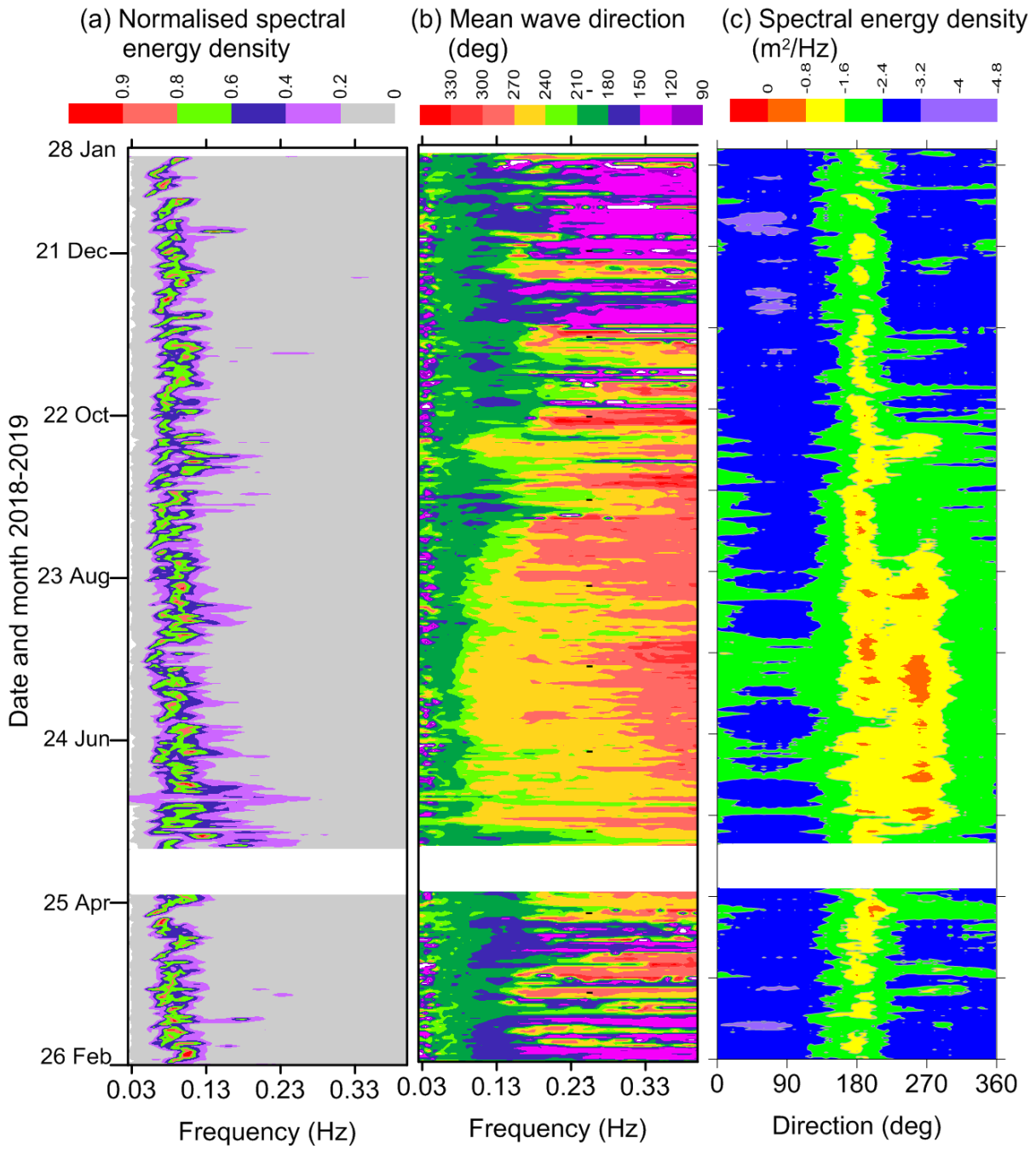


Figure 7. Contour plots of (a) normalized spectral density of the sea surface height variance, (b) mean wave direction, (c) contour plots of wave spectral energy density in logarithmic scale with direction and time during February 2018 to January 2019. Normalised spectral density of the sea surface height variance is obtained by dividing the spectral density at each frequency by the maximum spectral density of the sea surface height variance of the respective wave spectrum

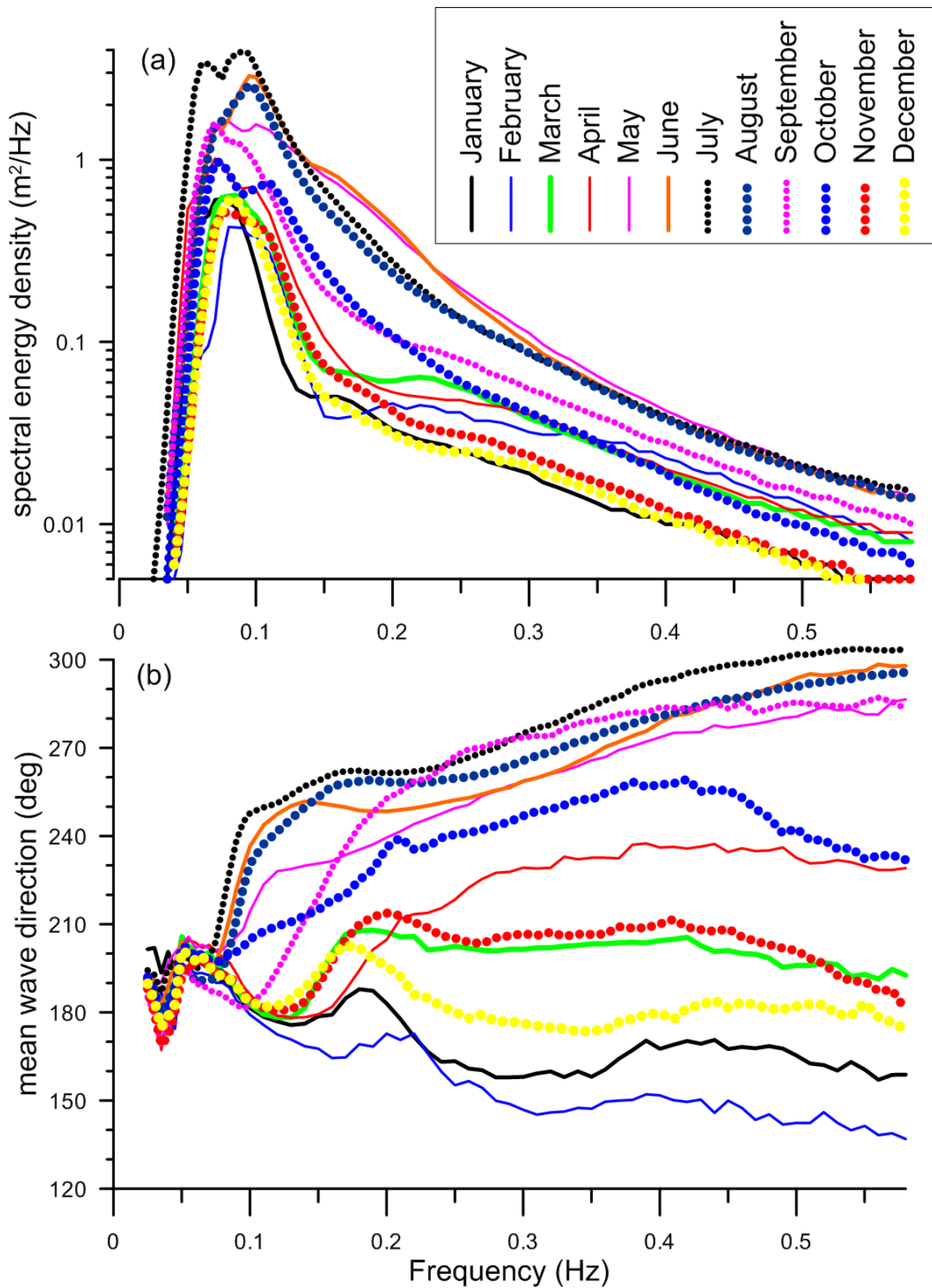


Figure 8. (a) Monthly average wave spectrum and (b) mean wave direction during February 2018 to January 2019

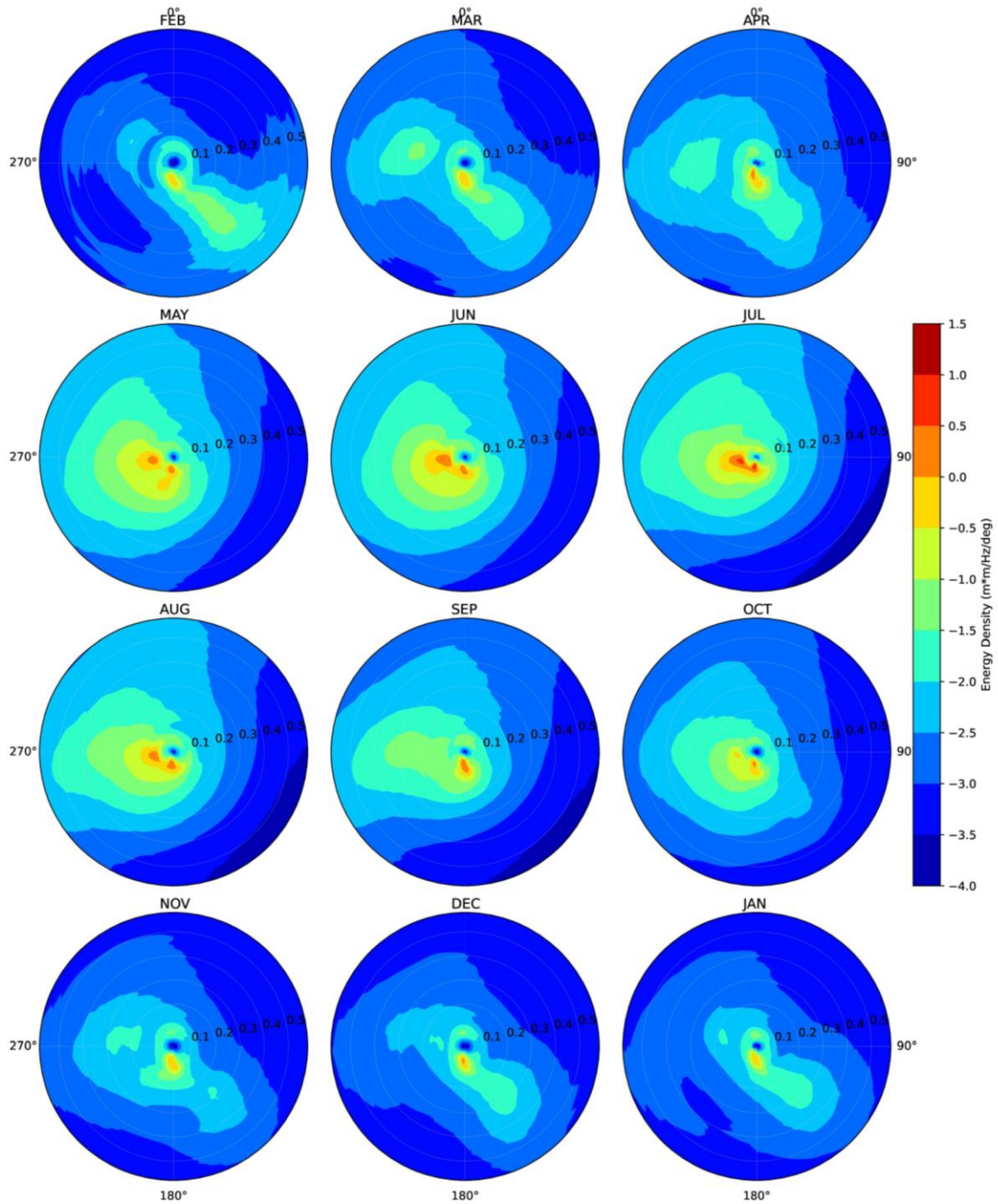


Figure 9. Monthly average directional wave spectrum for the period February 2018 to January 2019. The color bar is for spectral density ( $\text{m}^2 / \text{Deg}/\text{Hz}$ ). The spectral density of the sea surface height variance is shown in logarithmic scale (base 10)

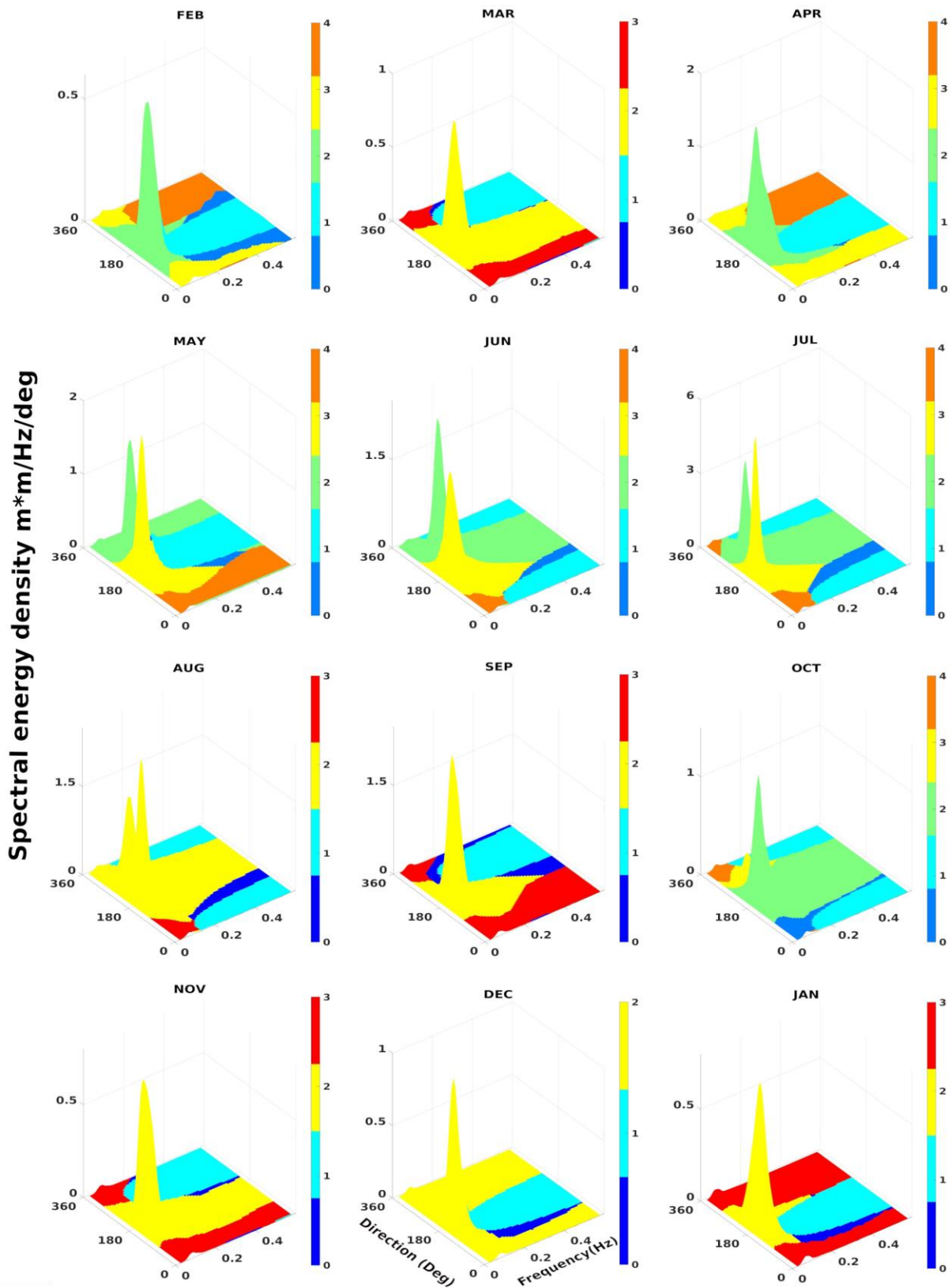


Figure 10. Wave spectral partitions in different months obtained from the monthly average directional spectra. The colour legend indicates the different wave systems present

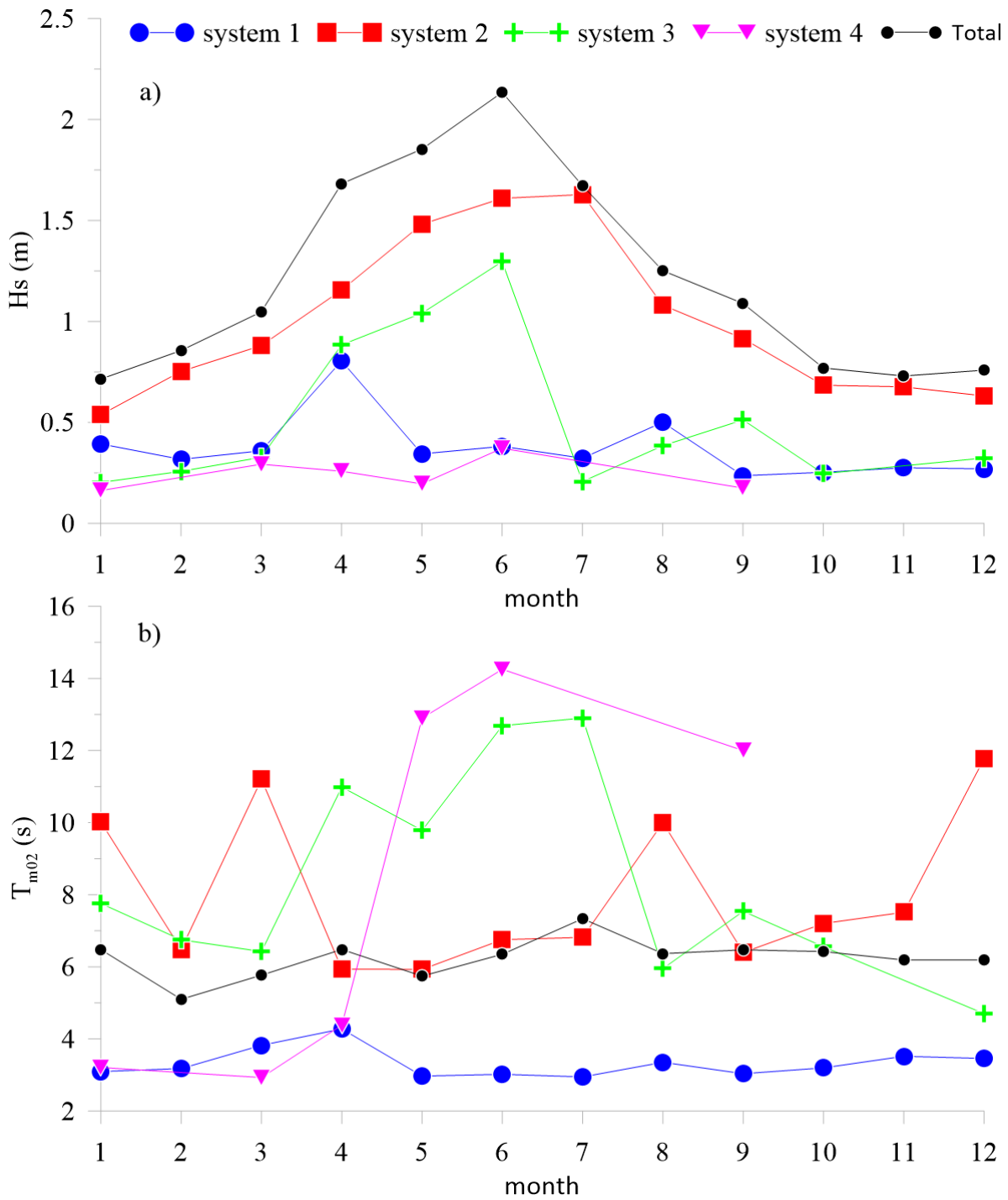


Figure 11. Monthly variation of system-wise significant wave height (a) and mean wave period (b) during February 2018 to January 2019